Avarmaa, Katri; Taskinen, Pekka; Klemettinen, Lassi; O'Brien, Hugh; Lindberg, Daniel

Ni–Fe–Co alloy – magnesia-iron-silicate slag equilibria and the behavior of minor elements Cu and P in nickel slag cleaning

Published in:
Journal of Materials Research and Technology

DOI:
10.1016/j.jmrt.2021.07.112

Published: 01/11/2021

Document Version
Publisher's PDF, also known as Version of record

Available online at www.sciencedirect.com

jmr&t Journal of Materials Research and Technology

journal homepage: www.elsevier.com/locate/jmrt

Ni–Fe–Co alloy – magnesia-iron-silicate slag equilibria and the behavior of minor elements Cu and P in nickel slag cleaning

Katri Avarmaa [a,c,*], *Pekka Taskinen* [a], *Lassi Klemettinen* [a], *Hugh O'Brien* [b], *Daniel Lindberg* [a]

[a] *Aalto University, School of Chemical Engineering, Department of Chemical and Metallurgical Engineering, P.O Box 16100, FI-00076 Aalto, Finland*

[b] *Geological Survey of Finland, Vuorimiehentie 2, 02150 Espoo, Finland*

[c] *Swinburne University of Technology, Department of Mechanical and Product Design Engineering, John Street, Hawthorn, Melbourne, Victoria, 3122, Australia*

ARTICLE INFO

Article history:
Received 24 March 2021
Accepted 24 July 2021
Available online 10 August 2021

Keywords:
Battery metals
Nickel processing
Reduction
LA-ICP-MS
Thermodynamic modelling

ABSTRACT

The increasing demand for metals and the tightening environmental restrictions on industries have led to a situation where improvements of new and existing process technologies for higher metal recoveries from primary and secondary resources are needed. This, in turn, requires a better understanding of process chemistry. The present study provides important fundamental information on the equilibrium reduction path and the formation of metal alloy in an electric furnace under nickel slag cleaning conditions, as well as the chemical properties of Ni, Co, Cu and P at these conditions. High-temperature equilibration experiments were conducted on magnesia-iron-silicate slags at silica saturation at 1400 °C (1637.15 K) and in the oxygen partial pressure range of 10^{-11}–10^{-7} atm (1.01325×10^{-6}–10^{-2} Pa). The samples were analyzed by electron microprobe (EPMA) for major and minor elements and laser ablation inductively coupled plasma mass spectrometer (LA-ICP-MS) for trace element compositions. Initially the slag contained 2 wt% Ni and 1 wt% Cu, Co and P each, added as oxides, and at $P_{O2} = 10^{-7}$ atm, these metals were only present in the slag with no metal alloy formed. At lower partial pressures, the alloy formed and its composition changed from 90wt-% Ni-rich to 50 wt-% Ni – 40 wt% Fe alloy as the P_{O2} decreased. Copper vaporized to a great extent at all conditions. The minor metals were shown to be present as NiO, $PO_{2.5}$, CoO and $CuO_{0.5}$ species in slag over the $P_{O2} = 10^{-8}$ -10^{-10} atm range.

* Corresponding author.
E-mail addresses: katri.avarmaa@aalto.fi, kavarmaa@swin.edu.au (K. Avarmaa).

https://doi.org/10.1016/j.jmrt.2021.07.112

1. Introduction

Circular economy, urban mining and sustainable metals processing are critical concepts for securing our metals supply. Currently, the metals used for electrical transportation and renewable energy solutions, such as cobalt and nickel, are facing sharply increasing demand requiring rapidly building up their production capacities in the near future. It is estimated that the demand for cobalt by 2030 will increase between 160 and 280 % from the world refinery capacity of 2016 [1], the nickel demand is forecasted to increase 215–350 % by 2050 [2] and copper between 275 and 350 % by 2050 [3]. With current technologies and resources, these production rates cannot be satisfied, but we need new innovations and technological solutions alongside improved processing of primary and secondary resources.

One important and critical process step in nickel processing to avoid significant losses of valuable metals, is the slag cleaning stage operated in an electric furnace. Recently, the trend has been towards higher matte grades (low-iron mattes) in the smelting stage, thus making the slag cleaning stage even more important. Copper and cobalt are typical valuable minor metals present in nickel sulfide ores and consequently in the feed concentrates [4], making their high recoveries especially important from the sustainability and smelter profitability point-of-views. In addition, phosphorus is a rather typical minor element in nickel ores and especially in ferronickel production based on nickel laterites [4]. Moreover, in Ni-bearing wastes, phosphorus is common element, especially in sludges from nickel plating [5]. The raw materials for nickel matte smelting have often lower sulfide content and higher MgO concentration compared to the copper smelting concentrates. Additionally, the slag cleaning stage has been shown to be a promising recycling process for Ni–Co-rich scraps [6], and thus its use for recycling purposes will most likely increase in the future.

Although the matte produced in nickel slag cleaning is chemically closer to a metal alloy, it is called electric furnace (EF) matte. The slags fed in the EF contain both mechanically entrained matte/metal droplets and chemically dissolved metals. Thus, appropriate reduction degree and sufficient settling time are key factors for the efficient recovery of metals. The aim of the process is to produce high-grade matte, i.e. high concentrations of Ni, Cu, Co and other valuable metals in EF matte, while keeping the iron concentration as low as possible. Nevertheless, due to similar chemical properties of cobalt and iron, some losses of valuable metals in slag and iron dissolution in matte are inevitable [7].

Literature on Ni, Cu and Co properties in matte/Ni alloy-slag systems under nickel smelting and converting conditions exist quite extensively. However, only a limited number of studies cover the reducing nickel slag cleaning conditions and have determined phosphorus properties in nickel processes. Moreover, previous studies have not utilized direct phase analysis techniques to measure the real chemical dissolutions of elements, but rather the bulk compositions including possible segregations of other phase(s). Table 1 collects previous experimental studies on nickel matte/alloy – iron-silicate slag systems investigating the distribution

Table 1 – Literature on Ni, Cu, Co and P distribution behavior in nickel alloy/matte - iron silicate slag systems.

Matte/alloy + other minors	Slag	Crucible	T/C	PO2/atm or matte grade	Reference
Ni–Fe + Cu, P, Co	FeO_x-SiO_2 + CaO	MgO	1400–1600	$10^{-9.5}$–10^{-6}	Pagador et al. [8,9]
Ni–Fe + Co/Cu	FeO_x-SiO_2-Al_2O_3	MgO	1500	$10^{-9.5}$–10^{-7}	Henao et al. [10]
Ni–Fe–Co	FeO_x-SiO_2	MgO	1500–1600	10^{-9}–10^{-1} (0–27 wt% Fe in alloy)	Li and Tsukihashi [11]
Cu–Ni–Fe + Co, P	FeO_x-SiO_2 + CaO	Fe and MgO	1300, 1400	10^{-11}–10^{-8} (1–12 wt%Fe in alloy)	Takeda et al. [12]
Ni–Cu–Fe–S + Co	FeO_x-SiO_2 + CaO, MgO, Al_2O_3	SiO_2	1250–1300	15–75 wt% Cu + Ni	Choi and Cho [13]
Ni–Fe–S/Ni–Fe–Cu–S/Ni–Cu–S + Co	FeO_x-SiO_2	MgO	1300	0–65 wt% Fe	Font et al. [14]
Ni–Fe–S + Co, Cu	FeO_x-SiO_2	MgO	1300	0–70 wt% Ni	Font et al. [15]
Ni–Cu–Fe–S	FeO_x-SiO_2	MgO	1300	0–75 wt% Ni + Cu	Font et al. [16]
Ni–Fe–S + Co	FeO_x-SiO_2	SiO_2	1250	5–60 wt% Fe	Lee [17]
Ni–Cu–Fe–S + Co	FeO_x-SiO_2-MgO	SiO_2	1350–1450	3–12 wt% Fe	Piskunen et al. [18]
Ni–Cu–Fe–S + Co	FeO_x-SiO_2	MgO	1250	1–20 wt% Fe	Toscano and Utigard [19]
Ni–Cu–Fe–S + Co	FeO_x-SiO_2 + K_2O, MgO	SiO_2	1400	2–8 wt% Fe	Sukhomlinov et al. [20]
Ni–Fe–S	FeO_x-SiO_2, FeO_x-CaO	MgO	1500	1–25 wt% Fe	Henao et al. [21]
Ni–Fe–S/Ni–Cu–Fe–S + Co	FeO_x-SiO_2 + MgO, Al_2O_3, CaO	SiO_2 and Al_2O_3	1250	0–70 wt% Ni (or Ni + Cu)	Celmer and Toguri [22]
Ni–Fe–S + Co	FeO_x-SiO_2		1300	20–75 wt% Ni	Computational study, Sorokin et al. [23,24]

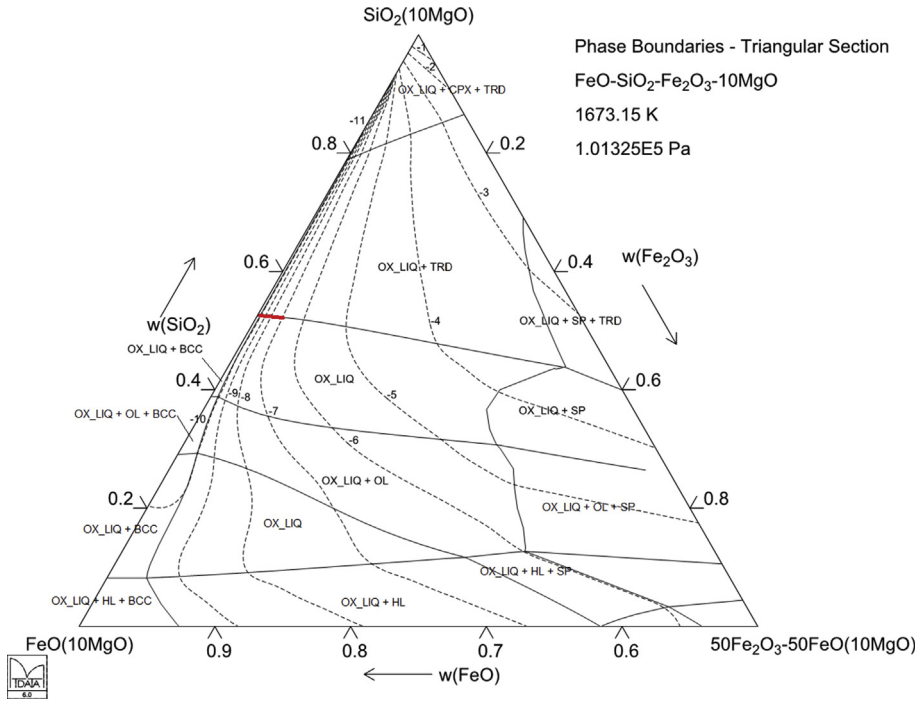

Fig. 1 – FeO–SiO_2–Fe_2O_3-10 wt% MgO phase diagram with $\log_{10}P_{O2}$ contours superimposed at 1400 °C. The red trend line represents the slag composition at tridymite saturation in the investigated P_{O2} range. The phase label abbreviations in the diagram: HL = halite, TRD = tridymite, SP = spinel, OL = olivine, OX_LIQ = oxide liquid and BCC = BCC-structured iron. (For interpretation of the references to color in this figure legend, the reader is referred to the Web version of this article.)

coefficients of Ni, Cu, Co and P at similar experimental conditions as those used in this study.

Additionally, some pilot scale experiments for industrial slags and industrial sampling trials on nickel processes have been performed. Jones et al. [7] executed pilot-plant test work at Mintek achieving recoveries of 98 % for nickel and over 80 % for cobalt, in the matte grade range from 10 to 65 wt% Fe and at 1500–1550 °C. Bustos et al. [25] executed converting simulations at Falconbridge limited and presented industrial results at a matte grade range of 0–35 wt% Fe. Additionally, Matusewicz and Mounsey [26] investigated cobalt, nickel and copper behavior in a pilot-scale Ausmelt furnace (100 kg/h) testing different process conditions (reverberatory furnace, converter and electric furnace). Furthermore, literature related to the PGM [27] and ferronickel smelting [28] cover the same metals, as especially Ni, Cu and Co are typical metals in PGM smelters and P is a critical element to be removed during the ferronickel process.

This study investigated the equilibrium between a sulfur-free, Ni-rich alloy and magnesia-iron-silicate slag in the oxygen partial pressure range of 10^{-11}–10^{-7} atm at 1400 °C, as well as the chemical properties of Ni, Cu, Co and P. The experiments were carried out employing a drop-quenching technique followed by direct spot analysis with electron microprobe and laser ablation inductively coupled plasma mass spectrometer [29] to quantify the phase compositions and determine the distribution coefficients, as well as further calculate the activity coefficients. MTDATA with the MTOX [30], TCFE and pure substance databases were used to predict slag equilibrium as well as to compare and interpret the experimental results.

2. Materials and methods

2.1. Thermodynamic calculations

MTDATA 6.0 with its MTOX [30] database was employed for calculating and predicting the slag equilibrium at different prevailing oxygen partial pressures. Figure 1 presents a phase diagram of FeO–SiO_2–Fe_2O_3-10wt%MgO system superimposed with oxygen activity (partial pressure) contours at 1400 °C.

According to the phase diagram calculated, the slag composition is expected to stay relatively similar in the P_{O2} range studied in this work. At the lowest investigated P_{O2} (10^{-11} atm), the system does not seem to reach the slag-tridymite boundary. The minor elements included in this study will slightly change these boundaries.

2.2. Experimental procedure and analytics

The experiments were conducted employing a well-developed drop-quench technique followed by electron probe micro-analysis (EPMA) and laser ablation inductively coupled plasma mass spectrometry (LA-ICP-MS). The experimental equipment

and procedure have been broadly presented in literature [31]. The equilibrium furnace employed was Nabertherm (Lilienthal, Germany) RHTV 120–150/18 with Nabertherm P310 temperature controller. Temperature was measured with a calibrated S-type Pt/90 %Pt–10 %Rh thermocouple (Johnson-Matthey, UK) and cold compensation junction by PT100 resistance thermometer (SKS Group, Finland) connected to 2010 DMM and 2000 DMM multimeters (Tektronix, Beaverton, USA), respectively. The data were measured in real time and logged with a Lab-view program.

The samples were equilibrated in $CO–CO_2$ gas mixtures corresponding to specific P_{O2} from 10^{-11} to 10^{-7} atm at 1400 °C, see Table 2. The flow rates were calculated based on the equilibrium constant value of the reaction $CO(g) + O_2(g) = CO_2(g)$. CO and CO_2 gas flows were controlled accurately by DFC26 thermal mass flow controllers (Aalborg, New York, USA). Argon gas was used for flushing the furnace post experiments. All gases were supplied by AGA-Linde (Finland) with purities >99.98 vol-%.

Table 3 shows all the solid materials employed in the experiments. Prior the slag mixture preparation, P_2O_5 and Fe_2O_3 were sintered with a P_2O_5/Fe_2O_3 (w/w) ratio = 1/3 for 10 min at 900 °C. These sintering conditions produced solid phases of $Fe_2P_2O_8 + Fe_6P_2O_{14}$ according to $P_2O_5–Fe_2O_3$ phase diagram by MTDATA-MTOX. The sintering was performed in order to avoid vaporization of phosphorus during the equilibrium experiments. The slag was prepared by weighing, crushing and mixing the materials in an agate mortar to a homogeneous powder mixture. The initial Fe/SiO_2 ratio of the slag was 0.82 (including FeO and Fe from the sintered $Fe_2O_3–P_2O_5$ pellet), MgO concentration 10 wt% and the concentrations of minor elements: NiO = 2.55 wt% (Ni = 2 wt%), Cu_2O = 2.26 wt% (Cu = 1 wt%), CoO = 1.27 wt% (Co = 1 wt%) and P = 1 wt% as sintered $Fe_2P_2O_8–Fe_6P_2O_{14}$ powder. Slag pellets weighing 0.2 g were pressed and used in the equilibrium experiments.

A slag pellet was equilibrated in a silica crucible (Heraeus 300 HQ glass, Finnish Special Glass, Espoo, Finland) for 18 h in controlled $CO–CO_2$ gas atmosphere at 1400 °C. The sample was quenched in ice water mixture and prepared, employing wet metallographic techniques, for SEM-EDS, EPMA and LA-ICP-MS analyses. Imaging and preliminary elemental composition analyses were conducted with Mira 3 SEM (Tescan, Brno, Czech Republic) equipped with an UltraDry Silicon Drift Energy Dispersive X-ray Spectrometer (EDS) supplied by Thermo Fisher Scientific (Waltham, MA, USA). The primary analyses were conducted employing an SX100 microprobe (Cameca SAS, France) equipped with five wavelength dispersive spectrometers (WDS), with an acceleration voltage of 20 kV and emission current of 15 nA. The beam size was for slag 100 μm and for metal 1–20 μm. The used standards were natural minerals and synthetic metals: Mg K_α and Si K_α (diopside), Fe K_α (hematite), Co K_α (cobaltite), O K_α (quartz), Ni K_α (Ni), Cu K_α (Cu) and P K_α (apatite). The detection limits of EPMA for slag and metal phases are presented in Table 4. Eight analysis points per phase were taken from each sample and used to calculate the concentration averages and standard deviations. The results were corrected employing a PAP on-line matrix correction program [32]. The totals were 100.5 ± 1.1 wt% for slag and 100.3 ± 0.8 wt% for metal. The sensitivity of EPMA for minor element measurements was sufficient, excluding for copper in slag and for phosphorus in metal alloy at 10^{-8} atm.

Due to the insufficient EPMA detection limits for Cu and P, both metal alloy and slag phases were analyzed by LA-ICP-MS. The slag phase was analyzed from all samples, and the metal alloy phase from four samples (one at each oxygen partial pressure between $10^{-11}–10^{-8}$ atm). The laser ablation system was equipped with a 193 nm ArF excimer laser (Teledyne CETAC Technologies, USA) and it was coupled to a single collector sector field ICP-MS (Nu Instruments Ltd, UK). The laser spot size was chosen as 50 μm, and the laser was fired at 10 Hz frequency with 2.17 J/cm^2 fluence on the sample surface. After 5 pre-ablation pulses, the gas background was analyzed for 20 s, followed by 400 (slag) or 300 (metal) laser pulses for signal acquisition. The mass spectrometer was operated in low resolution mode ($M/\Delta M = 300$), and data reduction was performed using the Glitter software [33].

For the slag phase, NIST 610 [34] standard reference material was used as the external standard. NIST 612 as well as USGS BHVO-2G and BCR-2G [35] glasses were analyzed as unknowns. Silicon (^{29}Si) was used as the internal standard, with concentration values from EPMA measurements. For the metal, UQAC FeS-1 pressed pellet [36] was used as the external standard, while USGS MASS-1 [37] sulfide as well as BHVO-2G and BCR-2G glasses were analyzed as unknowns. The internal standard was iron (^{57}Fe). The phosphorus concentration in UQAC FeS-1 was obtained by analyzing this material as an unknown, using BHVO-2G as the external standard and ^{57}Fe as the internal. The average value obtained for phosphorus was 120.8 ppm. In this work, the LA-ICP-MS concentration results were used for copper in the slag in all samples, and for phosphorus in the metal at 10^{-8} atm oxygen partial pressures.

Table 2 – The gas flow rates employed in the experiments (ml/min NTP).

$\log_{10}P_{O2}$	CO	CO_2
−7	41	259
−8	100	200
−9	184	116
−10	250	50
−11	282	18

3. Results

The alloy was formed during equilibration of the condensed phases with the prevailing gas atmosphere. Reduction and formation of the metal alloy from the oxide slag mixture were investigated as a function of oxygen partial pressure. Figure 2 shows the formation of the metal alloy in a micrographic sequence; in the highest P_{O2} no metal alloy was found, whereas as a function of decreasing P_{O2}, the amount of the alloy and the droplet size(s) seemed to increase. Based on the micrographs, the metal was formed as round-shaped droplet(s), indicative of liquid formed at the experimental temperature. Figure 3 presents high-magnification alloy micrographs at three different oxygen partial pressures. At $10^{-8}–10^{-9}$ atm, the alloys were entirely homogeneous (apart from some holes). When the P_{O2} decreased to 10^{-10} atm, a net

Table 3 – The solid reagent materials employed.

Chemical	Supplier	Purity (%)
FeO	Sigma–Aldrich	99.7
Fe_2O_3	Alfa Aesar	99.998
SiO_2	Umicore	99.99
MgO	Sigma–Aldrich	≥99
NiO	Sigma–Aldrich	99.99
CoO	Sigma–Aldrich	99.95
Cu_2O	Oxidized from copper cathode material (Boliden 99.999 %)	99.999
P_2O_5	Alfa Aesar	99.99

structure, visible as darker grey areas in the micrographs, appeared in the alloy and this net structure developed further at 10^{-11} atm.

Slag composition results based on EPMA measurements with their uncertainties (standard deviations ±1σ) are presented in Fig. 4. The composition of the slag, related to its Fe, SiO_2 and MgO concentrations, stays relatively constant, as predicted in the phase diagram in Fig. 1. A slight decrease in silica and magnesia concentrations as a function of increasing partial pressure was observed.

Figure 5 presents the concentration results of P, Co, Ni and Cu in slag as a function of P_{O2} with their uncertainties (±1σ). The P, Co and Ni concentrations were based on the EPMA measurements, and Cu concentrations were analyzed with the LA-ICP-MS.

At the highest oxygen partial pressure investigated, 10^{-7} atm, Ni, Co and P concentrations were close to their initial concentrations in the slag mixture. Figure 5 shows how nickel oxide started to reduce and form metal alloy at 10^{-8} atm. An especially large decrease in Ni concentration in slag occurred between 10^{-8} and 10^{-9} atm continuing to 10^{-10} atm with only 0.1 wt% of nickel dissolved in the slag. On the other hand, cobalt concentration exhibited only a small decrease between 10^{-7} and 10^{-9} atm, and the main decrease occurred when P_{O2} was decreased to 10^{-10} atm. However, even when the oxygen partial pressure was decreased to 10^{-11} atm, cobalt concentration in slag did not decrease below 0.4 wt%. Phosphorus concentration stayed constant around 1.1 wt% between 10^{-7} and 10^{-9} atm, and at more reducing conditions it decreased slightly down to 0.9 wt%. Copper concentration in the slag was very low throughout the entire investigated P_{O2} range, at maximum of 350 ppm at 10^{-7} atm (average of the repeated experiments), decreasing down to 50 ppm at 10^{-10} atm.

The metal alloy results with their uncertanties (±1σ) as a function of P_{O2} are presented in Fig. 6. Metal alloy did not form at 10^{-7} atm, but at 10^{-8} atm the alloy which formed was extremely rich in nickel (90 wt%Ni). As the P_{O2} decreased, the nickel concentration in the alloy decreased simultaneously with increasing iron, cobalt and phosphorus concentrations. Typical iron concentration in EF matte after slag cleaning is between 30 and 40 wt% [38]. The standard deviation of phosphorus was much greater than of the other elements, which can be explained by its tendency to form stable nickel phosphides that might have segregated during quenching. Moreover, at these concentration levels at 1400 °C, the Ni–P phase diagram showed a simultaneous existence of Ni alloy and liquid alloy [39] in a similar way as indicated by the TCFE database for Ni–Cu–Co–P alloys.

The alloy-slag system was investigated computationally with MTDATA employing its MTOX and TCFE databases. Special emphasis was placed on copper properties and its evaporation tendency since copper concentration in the alloy stayed constant at 0.4 wt% in the entire investigated P_{O2} range. As oxygen is not included in the TCFE database, all the oxygen carrier species in liquid alloy were excluded from the calculations. In the current experimental conditions, the solubility of oxygen is very small and thus no major error was caused in the equilibria by this simplification. Additionally, the alloy was forced into metastable liquid form as micrographs showing round-shaped droplets indicated to formation of a liquid phase. Different computations were carried out and their results and constrains are presented in the Supplementary file. The first calculation was done by varying the oxidation degree of the system (added O_2) i.e. as a function of partial pressure of oxygen at 1400 °C, wherein the gas volume flow rate (i.e. the gas/condensed phase ratio) was set to correspond the experimental conditions used. Because of the MTDATA user interface, the gas volume flow rate is presented as gas mass during the experiment. The gas mass was evaluated based on the densities of the gases (Ar, CO and CO_2) and their flow rates used in the experiments. Additionally, a calculation to examine the influence of the total gas volume (as mass of Ar) on copper vaporization was carrier out at constant $P_{O2} = 10^{-9.4}$ atm and T = 1400 °C by varying the gas mass from zero to the amount used in the experiments.

The computational results predicted that a metal alloy will form around 10^{-8} atm and below. The copper concentration was at a maximum of 1 wt% in the alloy and 0.05 wt% in the slag at 10^{-8} atm, whereas its partial pressure was relatively high at $10^{-5.7}$ atm and stayed constant throughout the investigated P_{O2} range. Copper was shown to be present almost fully in the gas phase (as Cu(g) species) as a function of P_{O2} and its gaseous species become dominant quickly when the gas mass increased. It was the only metal species whose partial pressure in gas and concentration in slag and metal showed a decreasing tendency when Ar mass, i.e. the gas mass/flow, increased in the system at constant

Table 4 – EPMA and LA-ICP-MS detection limits in ppmw.

	Mg	Si	Fe	Co	O	Ni	Cu	P
Slag	484	343	292	347	1294	331	455	194
Metal	819	402	259	394		443	578	222
Slag (laser)							^{65}Cu 0.01	
Metal (laser)								^{31}P 7.908

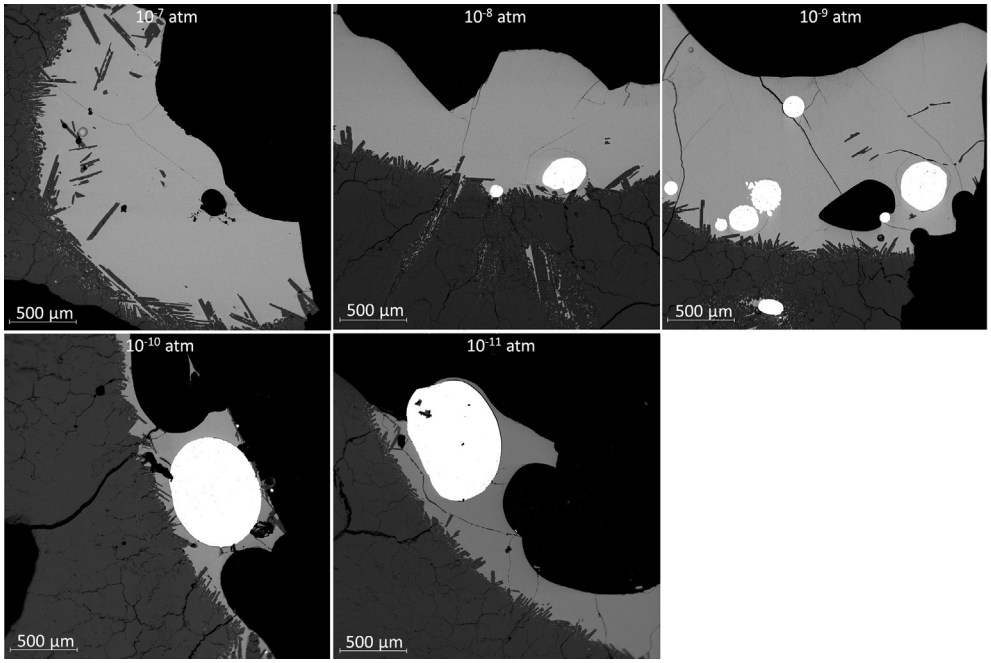

Fig. 2 – Microstructural formation and evolution of metal alloy as a function of decreasing oxygen partial pressure at 1400 °C.

$P_{O2} = 10^{-9.4}$ atm. The biggest difference between experimental and computational results was the iron concentration in the alloy at reducing conditions; MTDATA predicted approximately 90 wt% Fe at 10^{-11} atm and the experiments showed 35–40 wt%.

4. Discussion and conclusions

The recovery opportunities and removal efficiency of valuable metals Ni, Cu, Co and impurity element P in the slag cleaning process at different oxygen partial pressures were evaluated with distribution coefficients. In this study, the distribution coefficient was defined as the ratio of metal *M* in wt% between the nickel alloy *a* and slag *s*:

$$L^{a/s} = \frac{wt\%M_{alloy}}{(wt\%M)_{slag}} \quad (1)$$

The investigated metals were considered to dissolve in the slag via the following reaction:

$$M + x/2\ O_2\ (g) = MO_x \quad (2)$$

When the metal oxides are in monocationic form ($a_{MO} = y_{MO}N_{MO} = y_{MO}n_M/n_T$), the distribution coefficient can be presented in thermodynamic equilibrium by employing the equilibrium constant of reaction (2) and organizing the variables as follows:

$$L^{a/s}M = \frac{n_T(\gamma_{MOx})}{K(n_T)\gamma_M P_{O2}^{x/2}} \quad (3)$$

When the total number of moles n_T in 100 g alloy and (slag), as well as the activity coefficients γ in alloy and (slag) are constant, the slope of the curve for $\log_{10}L^{a/s}$ as a function of $\log_{10}P_{O2}$ reveals the oxidation degree of the metal *M*. The parantheses () in equations 1 and 3 indicate to slag phase.

The distribution coefficient is independent of scale of the system and thus applicable as such in industrial processes with corresponding conditions. On the other hand, it does not provide information on the element losses in gas, dust, fume or possible solids present/formed in the process, i.e. the overall recoveries. The distribution coefficients with trend

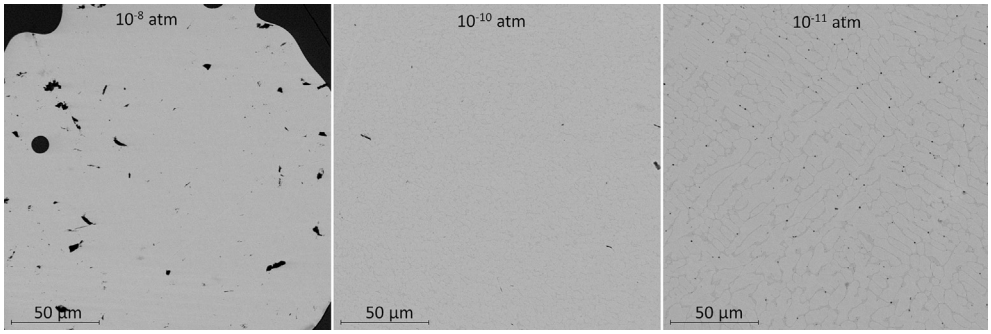

Fig. 3 – Microstructures of the alloys as a function of decreasing oxygen partial pressure.

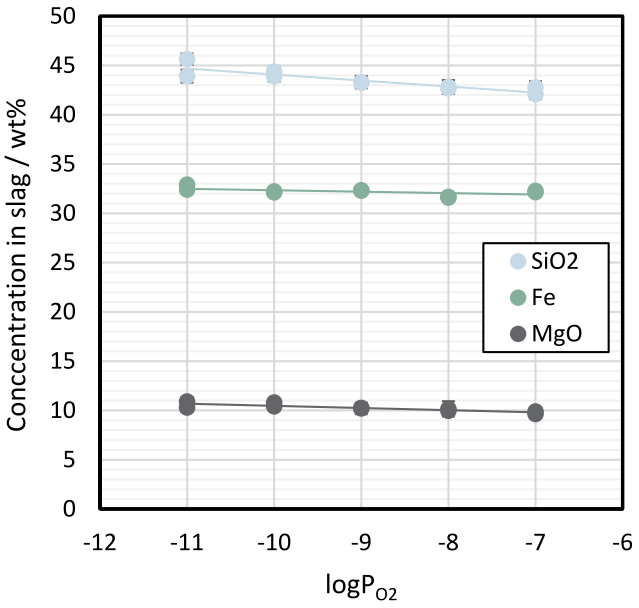

Fig. 4 – SiO_2, Fe and MgO concentrations in the slag as a function of P_{O2} at 1400 °C.

lines fitted in the P_{O2} range between 10^{-8} and 10^{-10} atm are presented in Fig. 7 (a). Additionally, equations for the trend lines are included to show the slopes of the curves; these indicate the oxidation degree of the elements in the slag. Figure 7 (b) shows the distribution results as a function of 'matte grade', i.e. the iron concentration in alloy.

The distribution coefficients for all the investigated minor elements decreased as the oxygen partial pressure, i.e. the matte grade increased (lower Fe in alloy), and the values were in the order Ni > Cu > Co > P. Nickel, copper and cobalt were distributed preferentially into the alloy after the alloy began to develop at 10^{-8} atm, whereas phosphorus distributed more into the slag above 10^{-10} atm P_{O2} and more into the metal, $L^{a/s}P = 2–3$, at $P_{O2} \leq 10^{-10}$ atm. The distribution coefficient of iron varied from 0.2 to 1.2 as a function of decreasing partial pressure of oxygen.

Nickel was recovered effectively in the alloy, as the value of the distribution coefficient $L^{a/s}$ was 60 at 10^{-8} atm, and it increased ten-fold, close to 600 at 10^{-10} atm. The slope of the trend line (0.5) strongly indicates divalent Ni^{2+}, i.e. NiO oxide form in the slag. Although copper vaporized to a great extent, the distribution coefficient $L^{a/s}$ Cu behaved as expected: copper preferred the alloy over slag, and the distribution coefficient increased as the conditions became more reducing. The slope of the trend line for copper (0.22) indicates monovalent Cu^{+}, i.e. $CuO_{0.5}$ form in the slag. Cobalt was also distributed more into the alloy, although presenting the lowest $L^{a/s}$ value of these three valuable metals. The slope (0.45) indicates divalent Co^{2+}, i.e. CoO form in the slag. Phosphorous distributed more into the slag above $P_{O2} = 10^{-10}$ atm, and slightly more into the alloy at $P_{O2} \leq 10^{-10}$ atm. The slope of the obtained curve (1.35) indicates pentavalent P^{5+} form as $PO_{2.5}$ species in the slag. All the indicated valences based on the trend line slopes are the most stable oxide forms considered in the literature.

Henao et al. [10] investigated the Ni-alloy and FeO_x-SiO_2-MgO-Al_2O_3 slag system with minor elements of Cu and Co at 1500 °C in the P_{O2} range 10^{-9}–10^{-7} atm. Their distribution coefficients for Ni, Cu and Co were one logarithmic order of magnitude higher than in our study. Additionally, Pagador et al. [8,9] investigated Ni/Ni–Cu alloy equilibrated with FeO_x-SiO_2-MgO slag with and without CaO addition at 1400–1600 °C in the P_{O2} range $10^{-9.5}$–10^{-6} atm. Their distribution results [9] for Ni and Co, at corresponding experimental conditions as in this study, are consistent with our results. The distribution coefficient of copper was around 100 at 10^{-9} atm and 1400 °C, being on the higher side of our results, whereas the value for phosphorus was somewhat lower in their study measured at 1500 °C [8]. They showed that the distribution coefficients of Cu, Ni, Co and P in Ni-alloy – FeO_x-SiO_2-MgO slag system increased when CaO and Al_2O_3 were added and when temperature increased [9,10]. Li and Tsukihashi [11] reported also Co and Ni distribution coefficients between Ni–Fe alloy and FeO_x-SiO_2-MgO slag at $P_{O2} = 10^{-9}$–10^{-1} atm and at 1500–1600 °C. Their results fit well with the results of Pagador et al. [8,9]. Takeda et al. [12] presented distribution coefficients for Cu, Ni, Fe, Co and P between Cu–Ni–Fe alloy and different iron-silicate and calcium ferrite slags at MgO or Fe saturation in the P_{O2} range 10^{-11}–10^{-8} atm (although only 0–12 wt% Fe in alloy) at 1300–1400 °C. Copper was a prevailing metal in the alloy, and their distribution coefficient results for Cu with fayalite slag were somewhat higher than in this study. The

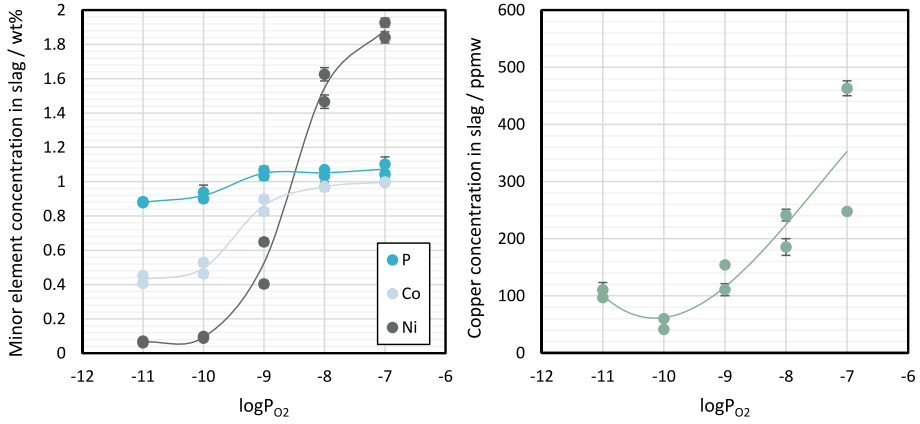

Fig. 5

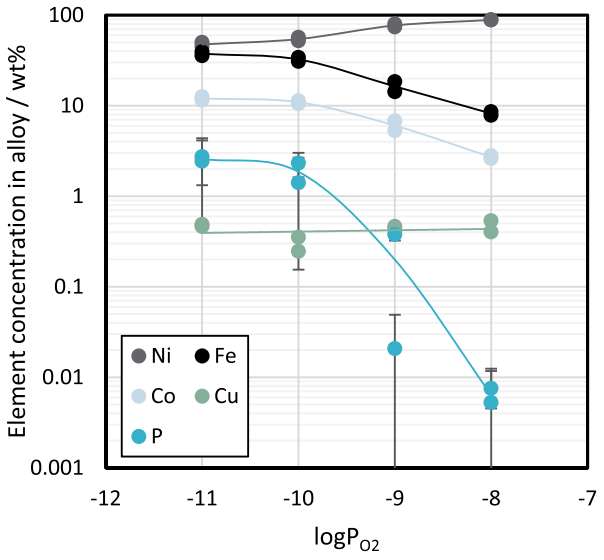

Fig. 6 – Metal alloy composition as a function P_{O2} at 1400 °C. The phosphorus concentration at 10^{-8} atm P_{O2} are from LA-ICP-MS, and the other results from EPMA measurements.

distribution coefficients of Ni and Co with fayalite slag were similar to ours in the reducing conditions and deviated increasingly as P_{O2} increased, whereas phosphorus distribution results at 1400 °C for fayalite slag fit with our results. All the distribution coefficients were greatly dependent on the slag type used in the experiments.

Font et al. presented the distribution coefficient of Co increasing from 1 to 10 as Cu–Ni matte grade increased from zero to 60 wt% Fe in matte [14] or decreased from 60 to 0 wt % Ni in matte [15] at 1300 °C, i.e. slightly lower than our results. Font et al. [15] presented the distribution coefficient of Cu changing from 15 to 30 as matte grade increased from 0 to 70 wt% Ni in matte at 1300 °C, which is slightly on the lower side compared to our results. Sukhomlinov et al. [40] investigated Co, Ni and Cu distributions in the copper-slag system and showed that the distribution coefficients $L^{Cu/s}$ of these metals increased as a function of increasing temperature, similarly as Choi and Cho [13] showed that temperature and additives influence the Co distribution coefficient. The results in the aforementioned studies were on same level in high matte grades, but differentiated increasingly as the process conditions became more reducing. Additionally, the results by Celmer & Toguri at 1250 °C seem to be on the lower side of our results. In general, the trend was that the previous Ni matte system results fit better with those presented here at oxidizing conditions but diverge at reducing conditions. It is also important to note, the comparison of metal-slag results in matte-slag studies where the matte grades are presented as wt% Ni or Ni–Cu in stead of wt% Fe is not straightforward.

Equation (3) was employed to evaluate the activity coefficients of minor element oxides (γ_{MOx}) in the slag. The average total moles (n_T) of slag in monocationic form per 100 g of slag were calculated as 1.61 ± 0.03 (1σ) and for alloy as 1.74 ± 0.03 (1σ). MTDATA-TCFE calculation for the alloy based on EPMA results in the partial pressure range 10^{-8}–10^{-10} atm at 1400 °C were executed to evaluate the activities and activity coefficients of elements (γ_M) in alloy. This P_{O2} range was chosen as the concentrations of metals in alloy varied almost linearly in these conditions and the (logarithmic) distribution coefficients and $\log_{10}P_{O2}$ were linearly associated between 10^{-8}–10^{-10} atm. The activity and activity coefficient results for the alloy in the third MTDATA calculation are shown in the Supplementary file.

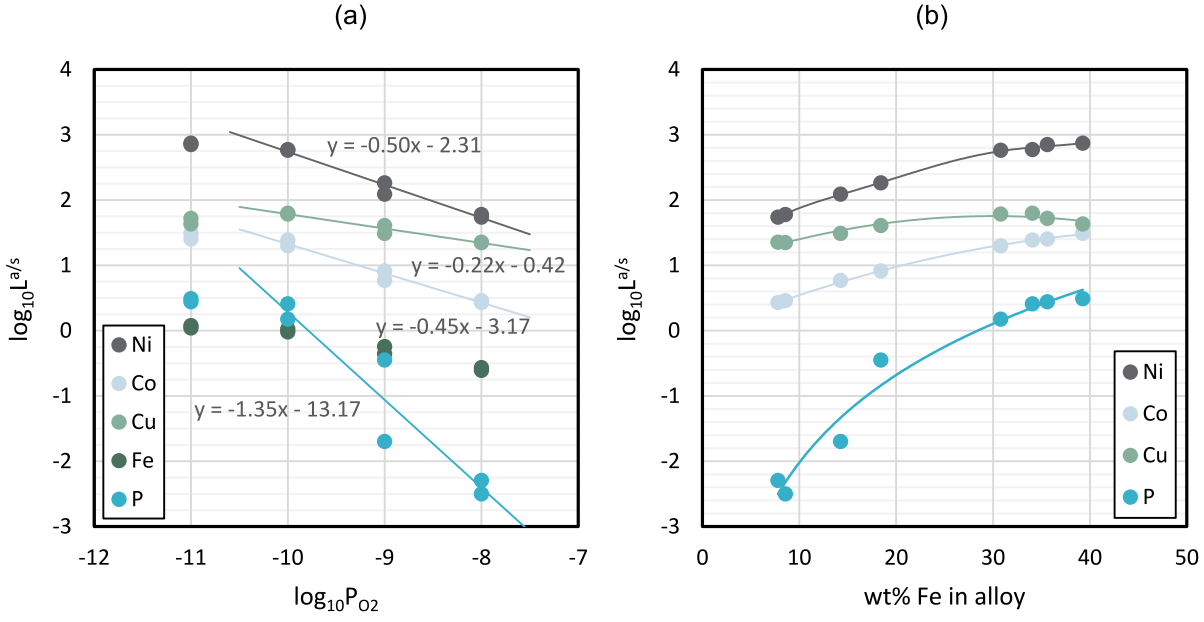

Fig. 7 – The distribution coefficients between alloy and slag obtained for Ni, Cu, Co and P as a function of P_{O2} (a) and matte grade (b) at 1400 °C.

Table 5 – The activity coefficients of mono-cationic oxides in slag (standard state: pure, liquid oxide).

$\log_{10}P_{O2}$	γCoO(l)	γNiO(l)	$\gamma PO_{2.5}$(l)	$\gamma CuO_{0.5}$(l)	γFeO(l)
−8	0.62	4.36	3.4E-07	2.20	1.12
−8	0.58	3.98	5.5E-07	3.09	1.02
−9	0.59	3.91	8.6E-06	2.70	1.12
−9	0.42	2.63	4.9E-07	1.65	0.87
−10	0.53	3.48	1.1E-05	1.24	0.81
−10	0.43	3.40	6.5E-06	2.30	0.73

The concentrations and activities of the elements in the metal alloy changed as a function of the partial pressure of oxygen. The Ni–Co–Fe system has been shown to behave close to an ideal system [41–44] and also the MTDATA calculations showed relatively constant behavior. Copper and phosphorus exist as minor elements in alloy, and thus should obey Henry's law, corroborated by their activity coefficients remaining close to constant. The activity coefficients of metals and their oxides always depend on the selected standard states. The reactions and standard states considered in this study were their pure liquid forms, as shown in the following equations (4)–(8):

$$Ni(l) + ½\ O_2(g) = NiO(l) \rightarrow \Delta G/kJ = -92.863 \rightarrow K = 7.932 \times 10^2 \quad (4)$$

$$Co(l) + ½\ O_2(g) = CoO(l) \rightarrow \Delta G^{\circ}/kJ = -106.546 \rightarrow K = 2.121 \times 10^3 \quad (5)$$

$$2Cu(l) + ½\ O_2(g) = Cu_2O(l) \rightarrow \Delta G^{\circ}/kJ = -48.943 \rightarrow CuO_{0.5}: K = 7.238 \quad (6)$$

$$2P(l) + 2.5O_2(g) = P_2O_5(l) \rightarrow \Delta G^{\circ}/kJ = -660.880 \rightarrow PO_{2.5}: K = 3.717 \times 10^{11} \quad (7)$$

$$Fe(l) + ½\ O_2(g) = FeO(l) \rightarrow \Delta G^{\circ}/kJ = -157.530 \rightarrow K = 8.287 \times 10^4 \quad (8)$$

The Gibbs energy change of the dissociation reactions of the general stoichiometric oxides to mono-cationic form was defined zero. Therefore, their K values can be evaluated employing general thermodynamic references, including the database of HSC 9.4.1 [45] as used in this study. As shown by Yazawa et al. [46], if expressing oxides in the mono-cationic form their activity coefficients remain close to constant over a large compositional range. They also showed that the total number of moles of species, (n_T) for typical non-ferrous smelting slags is almost constant in 100 g of slag with the mono-cation approach, as well as for mattes and alloys n_T. Although the activity coefficients of metals were relatively constant based on MTDATA-TCFE calculation, their accurate values shown in the Supplementary file were used to evaluate the activity coefficients of the oxides.

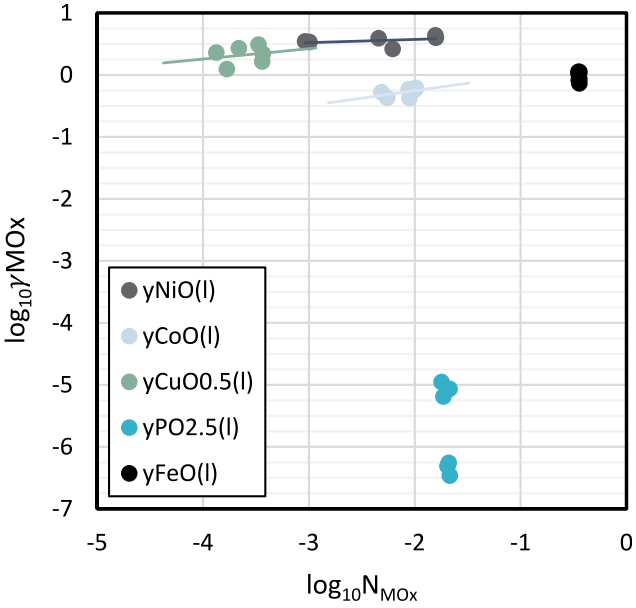

Fig. 8 – Activity coefficients of oxides as a function of N_{MOx}.

The activity coefficients of NiO(l), CoO(l), $CuO_{0.5}$(l), $PO_{2.5}$(l) and FeO(l) were calculated employing equation (3) and presented in Table 5 and in Fig. 8 as a function of molar fraction of the mono-cationic oxides (N_{MOx}).

Activity coefficients of the oxides were constant as a function molar fraction of the corresponding oxides, although the activity coefficients of cobalt and nickel oxides show a slight decrease as a function of oxygen partial pressure (Table 5). The activity coefficient of phosphorus oxide was very small, around 10^{-6}, i.e. deviating negatively from ideal behavior, also CoO(l) showed to a negative deviation from ideal behavior.

Lu et al. [47] investigated activity coefficients of NiO(s) and CoO(s) in $CaO–Al_2O_3–SiO_2$ slag and presented comprehensive literature review on previously presented activity coefficient values using pure solid standard states. The activity coefficient of NiO(l) calculated here was in the same level as in many other studies, whereas γ CoO(l) calculated by us was lower compared to other studies [47]. Based on the HSC, the K value for CoO, i.e. reaction (5) is more sensitive to the standard state used, liquid or solid, than NiO. The study by Takeda et al. [28] under ferronickel process conditions ($P_{O2} = 10^{-9}$ atm, $T = 1550$ °C) the activity coefficient of $PO_{2.5}$(l) was between 10^{-5}–10^{-6} depending on the slag composition. The activity coefficient of $CuO_{0.5}$(l) was lower than in the most comparable studies [8,10] in which also the distribution coefficient values were higher.

5. Conclusions

To improve the recoveries of valuable metals in existing and new process technologies, the chemical properties of target elements and the overall chemistry of the processes need to be better understood and accurately determined by experimentation. Only limited well-defined studies exist on the alloy formation in nickel EF slag cleaning. This study determined the distribution coefficients of Ni, Co, Cu and P between

forming Ni alloy and SiO_2-FeO_x-MgO slag based on true chemically dissolved element concentrations, measured with EPMA and LA-ICP-MS techniques. The systems were equilibrated under typical Ni-smelting and slag cleaning conditions in the oxygen partial pressure range of 10^{-11}–10^{-7} atm at 1400 °C.

In the most oxidizing conditions at 10^{-7} atm, no Ni-alloy formed. At lower oxygen partial pressures (10^{-11} –10^{-8} atm), the distribution coefficients between Ni-alloy and slag were determined, and the values were in the order Ni > Cu > Co > P. Copper showed a high tendency to vaporize from the system which could be deduced by its low initial concentration in slag at 10^{-7} atm and by the computational results of MTDATA. The investigated elements were shown to be present as NiO, $CuO_{0.5}$, CoO and $PO_{2.5}$ species in the slag in the oxygen partial pressures between 10^{-8} and 10^{-10} atm. Additionally, their activity coefficients in the slag were calculated using solution thermodynamics based on the experimental results and available thermodynamic data (MTDATA-TCFE and HSC).

Declaration of Competing Interest

The authors declare that they have no known competing financial interests or personal relationships that could have appeared to influence the work reported in this paper.

Acknowledgements

The study received financial support from the BATCircle (grant 4853/31/2018) by Business Finland. Lassi Klemettinen is grateful for the doctoral study grant provided by the Finnish Steel and Metal Producers' Fund and the funding provided by Aalto University School of Chemical Engineering. This study utilized the Academy of Finland's RawMatTERS Finland Infrastructure (RAMI) based at Aalto University, GTK and VTT in Espoo. Mia Tiljander at Geological Survey of Finland is greatly appreciated for conducting the EPMA analyses.

Appendix A. Supplementary data

Supplementary data to this article can be found online at https://doi.org/10.1016/j.jmrt.2021.07.112.

REFERENCES

[1] Fu X, Beatty DN, Gaustad GG, Ceder G, Roth R, Kirchain RE, et al. Perspectives on cobalt supply through 2030 in the face of changing demand. Environ Sci Technol 2020;54:2985–93.
[2] Elshkaki A, Reck BK, Graedel T. Anthropogenic nickel supply, demand, and associated energy and water use. Resour Conserv Recycling 2017;125:300–7.
[3] Elshkaki A, Graedel T, Ciacci L, Reck BK. Copper demand, supply, and associated energy use to 2050. Global EnvironChange 2016;39:305–15.
[4] Crundwell F, Moats M, Ramachandran V, Robinson T, Davenport WG. Extractive metallurgy of nickel, cobalt and platinum group metals. Oxford, UK and Amsterdam, the Netherlands: Elsevier; 2011.
[5] Nakajima K, Daigo I, Okada K, Koike S, Nansai K, Matsubae K, et al. Bottlenecks in material cycle of nickel. Matériaux Tech 2016;104:604.
[6] Avarmaa K, Järvenpää M, Klemettinen L, Marjakoski M, Taskinen P, Lindberg D, et al. Battery scrap and biochar utilization for improved metal recoveries in nickel slag cleaning conditions. Batteries 2020;6:58.
[7] Jones R, Hayman D, Denton G. Recovery of cobalt, nickel, and copper from slags, using DC-arc furnace technology. Pyrometallurg Div 1998;2125:1–17.
[8] Pagador RU, Hino M, Itagaki K. Distribution of minor elements between MgO saturated FeO_x–MgO–SiO_2 or FeO_x–CaO–MgO–SiO_2 slag and nickel alloy. Mater Trans JIM 1999;40:225–32.
[9] Pagador RU, Hino M, Itagaki K. Solubility of Ni, Cu and minor elements in FeO_x-SiO_2-MgO slag equilibrating with nickel alloy. In: Proceedings of the Fifth molten slags, fluxes and salts conference, Sydney, Australia. Warrendale, PA: The Society; 1997. p. 321–7.
[10] Henao HM, Hino M, Itagaki K. Distribution of Ni, Cr, Mn, Co and Cu between Fe-Ni alloy and FeO_x-MgO-SiO_2 base slags. Mater Trans 2001;42:1959–66.
[11] Li G, Tsukihashi F. Distribution equilibria of Fe, Co and Ni between MgO-saturated FeO_x–MgO–SiO_2 slag and Ni alloy. ISIJ Int 2001;41:1303–8.
[12] Takeda Y, Kanesaka S, Yazawa A. Equilibria between FeO_x-CaO-SiO2 slag and liquid Cu-Ni-Fe alloy. In: Proceedings of CIM 25th annual conference of metallurgists. Toronto: Canada; 1986. p. 185–202.
[13] Choi N, Cho W. Distribution behavior of cobalt, selenium, and tellurium between nickel-copper-iron matte and silica-saturated iron silicate slag. Metall Mater Trans B 1997;28:429–38.
[14] Font J, Hino M, Itagaki K. Phase equilibrium between FeO_x-SiO_2 base slag and Cu_2S-Ni_3S_2-FeS mattes with different Cu and Ni Contents at 1573 K. Shigen Sozai 1999;115:460–5.
[15] Font JM, Hino M, Itagaki K. Minor elements distribution between iron-silicate base slag and Ni_3S_2–FeS matte under high partial pressures of SO_2. Mater Trans JIM 1998;39:834–40.
[16] Font JM, Hino M, Itagaki K. Phase equilibrium and minor elements distribution between iron-silicate base slag and nickel-copper-iron matte at 1573 K under high partial pressures of SO_2. MaterTransJIM 1999;40:20–6.
[17] Lee WP. The thermodynamic behavior of magnetite in non-ferrous smelting. Doctoral thesis. University of Toronto, Department of Metallurgy and Materials Science; 1999. p. 204.
[18] Piskunen P, Avarmaa K, O'Brien H, Klemettinen L, Johto H, Taskinen P. Precious metal distributions in direct nickel matte smelting with low-Cu mattes. Metall Mater Trans B 2018;49:98–112.
[19] Toscano P, Utigard A. Nickel, copper, and cobalt slag losses during converting. Metall Mater Trans B 2003;34:121–5.
[20] Sukhomlinov D, Klemettinen L, Virtanen O, Lahaye Y, Latostenmaa P, Jokilaakso A, et al. Trace element distributions between matte and slag in direct nickel matte smelting. CanMetallQ 2020;59:67–77.
[21] Henao HM, Hino M, Itagaki K. Phase equilibrium between Ni-S melt and FeO_x-SiO_2 or FeO_x-CaO based slag under controlled partial pressures. Mater Trans 2002;43:2219–27.
[22] Celmer R, Toguri J. Cobalt and gold distribution in nickel-copper matte smelting. Nickel Metallurgy 1986;1:147–63.
[23] Sorokin ML, Nikolaev G, Komkov A. Slag cleaning operation in nickel production, Co-products and minor elements in non-ferrous smelting. In: Proceedings of the TMS annual meeting,

Las Vegas, Nevada, U.S.; Theo Lehner; minerals. Warrendale, Pa., U.S.: Metals & Materials Society; 1995. p. 67–78.
[24] Sorokin M, Nikolaev A. Behavior of cobalt during nickel concentrates processing. Russ J Non-Ferrous Metals 1994;35:11–5.
[25] Bustos A. Converting simulation at Falconbridge limited. Extractive metallurgy of nickel and cobalt; 1988. p. 335–54.
[26] Matusewicz R, Mounsey E. Using ausmelt technology for the recovery of cobalt from smelter slags. J Miner Met Mater Soc 1998;50:53–6.
[27] Andrews L, Pistorius P. Nickel, copper and cobalt distribution and equilibria in Anglo Platinum furnace slags. Miner Process Extr Metall (IMM Trans Sect C) 2010;119:52–9.
[28] Takeda O, Lu X, Miki T, Nakajima K. Thermodynamic evaluation of elemental distribution in a ferronickel electric furnace for the prospect of recycling pathway of nickel. Resour Conserv Recycling 2018;133:362–8.
[29] Avarmaa K, O'Brien H, Johto H, Taskinen P. Equilibrium distribution of precious metals between slag and copper matte at 1250–1350 C. J Sustain Metallurgy 2015;1:216–28.
[30] Gisby J, Taskinen P, Pihlasalo J, Li Z, Tyrer M, Pearce J, et al. MTDATA and the prediction of phase equilibria in oxide systems: 30 years of industrial collaboration. Metall Mater Trans B 2017;48:91–8.
[31] Avarmaa K, Klemettinen L, O'Brien H, Taskinen P. Urban mining of precious metals via oxidizing copper smelting. Miner Eng 2019;133:95–102.
[32] Pouchou J, Pichoir F. Basic expression of "PAP" computation for quantitative EPMA. In: Proceedings of the 11th international congress on X-ray optics and microanalysis (ICXOM), London, ontario, Canada. vol. 11. ICXOM; 1987. p. 249–56. J.D. Brown and R.H. Packwood.
[33] Van Actherbergh E. Data reduction software for LA-ICP-MS. In: Laser Ablation-ICP-mass spectrometry in the earth sciences: principles and applications; 2001. p. 239–43.
[34] Jochum KP, Weis U, Stoll B, Kuzmin D, Yang Q, Raczek I, et al. Determination of reference values for NIST SRM 610–617 glasses following ISO guidelines. Geostand Geoanal Res 2011;35:397–429.
[35] Jochum KP, Willbold M, Raczek I, Stoll B, Herwig K. Chemical characterisation of the USGS reference glasses GSA-1G, GSC-1G, GSD-1G, GSE-1G, BCR-2G, BHVO-2G and BIR-1G using EPMA, ID-TIMS, ID-ICP-MS and LA-ICP-MS. Geostand Geoanal Res 2005;29:285–302.
[36] UQAC FeS-1 pressed sulfide pellet composition. https://sulfideslasericpms.wordpress.com/rm-available/. [Accessed 2 February 2021].
[37] Wilson S, Ridley W, Koenig A. Development of sulfide calibration standards for the laser ablation inductively-coupled plasma mass spectrometry technique. J Anal At Spectrom 2002;17:406–9.
[38] Warner A, Diaz C, Dalvi A, Mackey P, Tarasov A, Jones R. JOM world nonferrous smelter survey Part IV: nickel: Sulfide. J Occup Med 2007;59:58–72.
[39] Schmetterer C, Vizdal J, Ipser H. A new investigation of the system Ni–P. Intermetallics 2009;17:826–34.
[40] Sukhomlinov D, Klemettinen L, Avarmaa K, O'Brien H, Taskinen P, Jokilaakso A. Distribution of Ni, Co, precious, and platinum group metals in copper making process. Metall Mater Trans B 2019;50:1752–65.
[41] Cacciamani G, Dinsdale A, Palumbo M, Pasturel A. The Fe–Ni system: thermodynamic modelling assisted by atomistic calculations. Intermetallics 2010;18:1148–62.
[42] Fraser DG, Rammensee W. Activity measurements by Knudsen cell mass spectrometry—the system Fe-Co-Ni and implications for condensation processes in the solar nebula. Geochim Cosmochim Acta 1982;46:549–56.
[43] Riani P, Sufryd K, Cacciamani G. Critical assessment and experimental investigation of Co–Ni–Ti phase equilibria. Calphad 2014;44:26–38.
[44] Wang J, Lu X, Zhu N, Zheng W. Thermodynamic and diffusion kinetic studies of the Fe-Co system. Calphad 2017;58:82–100.
[45] Roine A. HSC chemistry software, outotec, Pori software. 2018. available at: www.outotec.com/HSC.
[46] Yazawa A, Nakazawa S, Takeda Y. Distribution behavior of various elements in copper smelting systems. Adv Sulfide Smelt 1983;1:99–117.
[47] Lu X, Miki T, Nagasaka T. Activity coefficients of NiO and CoO in CaO–Al 2 O 3–SiO 2 slag and their application to the recycling of Ni–Co–Fe-based end-of-life superalloys via remelting. Int J Miner Metall Mater 2017;24:25–36.

Dr. Katri Avarmaa is currently a postdoctoral research fellow at Swinburne University of Technology, Australia. She obtained her MS and BS degrees in Materials Technology from Aalto University in Finland and completed her Ph.D. degree in Processing of Materials at Aalto University in 2019. Her research focus includes pyrometallurgical processing, chemical thermodynamics and circular economy or metals. Katri has 30 peer-reviewed journal publications and 10 conference papers.

Dr. Pekka Taskinen was appointed as a full professor of thermodynamics and modelling at HUT (Helsinki University of Technology) in 2008 (from 2010 onwards Aalto University). Professor Taskinen held adjunct professor positions in HUT and Oulu University since 1982 and 1991, respectively, and a guest professorship at Central South University (CSU) in China 2013-2017. He held several industrial R&D positions in Outokumpu Group (later Outotec) since 1983 until 2008. He has PhD degree in Theoretical Process Metallurgy from HUT (1981) and was as post-doc at Max Planck Institut in 1981. He has published more than 260 publications in peer-reviewed Journals and 180 Conference publications. In addition, he is author in 55 public technical reports, 56 workshop and professional magazine publications. He has 20 patents. His educational activities include lectures in thermodynamics, smelting technologies and related seminars. During his 9 years professor career he educated 19 PhD candidates to defence, and 3 out of those were double degrees with CSU. Since his retirement at Aalto University in 2017, he has acted as consultant for international and local companies, and supervisor of academic theses. He acts as peer reviewer in several high-reputation Journals in the field of thermodynamics and metals processing with the current rate of 50-70 manuscripts pa.

Lassi Klemettinen is a Ph.D. student at Aalto University in Finland. He obtained his Master's degree from Aalto University in the field of Functional Materials in 2017. His research focuses on the behavior of trace elements in copper smelting processes, with special emphasis on characterization techniques. Lassi has 36 peer-reviewed journal publications and 9 conference papers.

Dr. Hugh O'Brien is a senior research scientist in the Research Laboratory of the Geological Survey of Finland. He received his Ph.D. in 1988 based on the petrology and geochemistry of a suite of potassic volcanic and intrusive rocks in central Montana. His current research centers around trace element and isotope studies of rock and ore minerals using electron beam and laser ablation ICP mass spectrometry techniques. Applying these same spot analytical techniques to experimental charges on secondary

ores in a new direction of research, yet a natural extension of the capabilities of these techniques. He has 88 publications in peer-reviewed Journals, 78 conference papers, and an h-index of 23.

Dr. Daniel Lindberg is an Associate professor in Thermodynamics of Metallurgical Processes at Aalto University, School of Chemical Engineering. He attained his Doctor of Science degree in Inorganic Chemistry and his MSc degree in Geology and Mineralogy at Åbo Akademi University, Finland. His research focuses on chemical thermodynamics of high-temperature industrial inorganic chemistry, with focus on ash and corrosion chemistry in combustion processes, as well as pyrometallurgical processes. He also works on determining thermodynamic properties of inorganic compounds in these processes.